POLITECNICO DI TORINO
Repository ISTITUZIONALE

A high-efficiency portable system for insulation condition assessment of wind farm inter-array cables with double-sided partial discharge detection and localisation

Original
A high-efficiency portable system for insulation condition assessment of wind farm inter-array cables with double-sided partial discharge detection and localisation / Yan, Y; Zhao, Ys; Zhao, K; Trinchero, R; Stievano, Is; Li, Hj. - In: IET GENERATION, TRANSMISSION & DISTRIBUTION. - ISSN 1751-8687. - ELETTRONICO. - 17:11(2023), pp. 2523-2534. [10.1049/gtd2.12834]

Availability:
This version is available at: 11583/2979412 since: 2023-06-16T14:22:34Z

Publisher:
INST ENGINEERING TECHNOLOGY-IET

Published
DOI:10.1049/gtd2.12834

Terms of use:

This article is made available under terms and conditions as specified in the corresponding bibliographic description in the repository

Publisher copyright

(Article begins on next page)

07 May 2026

IET Generation, Transmission & Distribution

Special issue

Call for Papers

Be Seen. Be Cited.
Submit your work to a new IET special issue

Connect with researchers and experts in your field and share knowledge.

Be part of the latest research trends, faster.

Read more

The Institution of Engineering and Technology

Check for updates

Received: 21 October 2022 | Revised: 23 February 2023 | Accepted: 16 March 2023

IET Generation, Transmission & Distribution

DOI: 10.1049/gtd2.12834

ORIGINAL RESEARCH

A high-efficiency portable system for insulation condition assessment of wind farm inter-array cables with double-sided partial discharge detection and localisation

Yuan Yan[1,2] | Yinsong Zhao[1] | Kun Zhao[1,2] | Riccardo Trinchero[2] | Igor Simone Stievano[2] | Hongjie Li[1]

[1]The School of Electrical Engineering, Xi'an Jiaotong University, Xi'an, China

[2]The Department of Electronics and Telecommunications, Politecnico di Torino, Turin, Italy

Correspondence
Riccardo Trinchero, The Department of Electronics and Telecommunications, Politecnico di Torino, Turin, Italy.
Email: riccardo.trinchero@polito.it

Funding information
China Scholarship Council

Abstract

Partial discharge (PD) diagnosis is a crucial tool to assess the insulation condition of wind farm cables. Among PD diagnosis techniques, PD localisation is promising as it can provide target maintenance indicators on the insulation weak points of the cables. Accordingly, this paper developed a portable PD detection and location system for wind farm inter-array cables. The system consists of two non-invasive and lightweight testing units, which can be conveniently deployed on an energised cable, enabling highly efficient online PD diagnosis of the widely distributed inter-array cables. The system achieves accurate PD localisation of the energised cable via an improved double-sided travelling wave method. The method exhibits two superior features: the double-sided testing units are accurately synchronised via the joint application of Global Position Systems and a pulse-based interaction process, and a windowed phase difference method is proposed and integrated into the system to robustly estimate the time-of-arrival difference in low signal-to-noise ratio environment. Validation experiments were conducted on both a 10-kV cable in the laboratory and a real 35-kV cable in an on-shore wind farm.

1 | INTRODUCTION

1.1 | Background

The number of wind farms has substantially increased in recent years with the increasing global demand for renewable energy. In wind farms, inter-array medium voltage (MV) cables are fundamental to transmitting the power from turbines to high-voltage substations. Experiences of the last 20 years have shown that MV cables are the largest contributor to power failures in wind farms [1]. Wind farm operators continue to increase investment in improved tools to collect accurate and detailed information on the condition and performance of the MV cable networks to maintain their high reliability and availability [2]. This strategy is known as condition-based maintenance [3, 4].

Partial discharge (PD) diagnosis is a sensitive tool in condition-based maintenance of MV cables as it directly reveals the insulation deterioration degree of the cables, which has proven to be the main cause of most cable failures [5, 6]. According to the standard IEEE 400.4 [7], offline PD diagnosis of MV cables is required in their commissioning phase by energising the cables with a damped alternating current voltage. The technique has proven useful in ensuring the integrity of the cables [8, 9]. However, recently some researchers [10, 11] pointed out that PD activities in MV cables are a dynamic physical phenomenon related to temperature, electrical stress, ambient conditions and mechanical stress factors. This causes the offline PD diagnosis technique to be insufficient to cover the entire life cycle of the cables. As an alternative solution, online PD diagnosis of MV cables has demonstrated its special superiority of flexibility, timeliness and no need to de-energise the cables [4, 12, 13]. In the online PD diagnosis process, PD localisation is an essential step as it provides the exact location information of the PD source, improving the efficiency of

This is an open access article under the terms of the Creative Commons Attribution License, which permits use, distribution and reproduction in any medium, provided the original work is properly cited.
© 2023 The Authors. *IET Generation, Transmission & Distribution* published by John Wiley & Sons Ltd on behalf of The Institution of Engineering and Technology.

subsequent maintenance actions. However, achieving accurate online PD localisation of MV cables remains challenging, primarily due to synchronisation problems and field noisy interferences.

1.2 | Related work

The travelling wave method is the most commonly used approach for PD localisation of power cables [14–22]. It is mainly divided into two categories: single-sided [14] and double-sided methods [15]. Since an energised cable is always connected to others and the reflection at the remote side would be very weak, the single-sided PD location method can only perform satisfactorily on very short cables. In contrast, the double-sided method does not have such a problem and is more suitable for online PD localisation. Nevertheless, the difficulty in synchronising the PD detectors at double sides has posed a challenge for the double-sided location method. Global position system (GPS) is the most widely used, but its synchronisation precision fluctuates and is very susceptible to environmental factors, for example, weather and the surrounding geography. In [16], inspired by the power carrier communication technique, an alternative synchronisation approach was proposed for cable PD localisation based on pulse injection and the approach is further improved in [17, 18]. However, the survey in [19] showed that the in-field reliability of this pulse synchronisation approach sometimes might fail, particularly in noisy environments where the noise levels are as high as the injected pulses.

Different kinds of electromagnetic interferences can significantly reduce the PD localisation accuracy by influencing the determination of the accurate time-of-arrivals of the PD pulses in online PD measurement. In [20], representative time-of-arrival estimate methods were summarised for PD localisation of cables, and the energy criterion and phase difference methods were shown to be more accurate than the threshold method, Akaike information criterion and Gabor centroid method. In [21], the energy criterion method was also proven to be more accurate than the peak method, considering the high-frequency attenuation and dispersion characteristics of the PD signals in cables. In [22], the phase difference method was successfully applied in the single-sided PD localisation of cables. All the above-presented methods did not deal with noise problems, so they may fail to be applied for online PD localisation in wind farms cables as various noises may couple to the cables from the controlling and switching devices in wind turbines. These noises mainly include discrete spectrum noise and white noise [23]. Discrete spectrum noise mainly arises from carrier communication, radio communication, high-order harmonic etc., whilst white noise is mainly caused by equipment thermal noise, ground noise, rand noise etc. [24].

1.3 | Contribution and paper organisation

The current study was motivated by the limitations of the above-mentioned methods for PD localisation, offering the following main contributions and improvements.

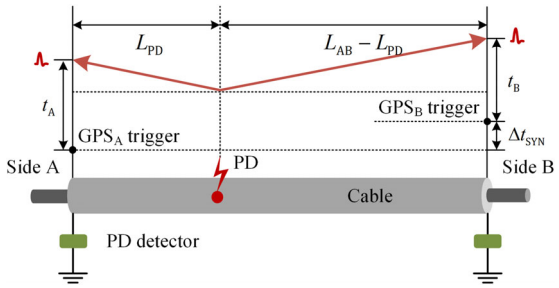

FIGURE 1 The classical double-sided partial discharge (PD) location method.

1. An improved online double-sided PD location method is developed. Reliable synchronisation of the double-sided PD detectors is achieved by the joint application of GPSs and a pulse-based interaction process.
2. A windowed phase difference method is proposed to estimate the time-of-arrival difference between the PD pulses collected by the PD detectors at the double sides of the cable. It is proven to be effective in a low signal-to-noise ratio environment.
3. A portable PD detection and location system is developed based on the methods proposed above. Its effectiveness and feasibility were validated through laboratory and field experiments.

The rest of this paper is structured as follows; Section 2 formulated the improved double-sided PD location method. In Section 3, the windowed phase difference method is proposed. In Section 4, the portable PD location system is implemented. In Section 5, laboratory validation of the developed methods and system is thoroughly discussed. In Section 6, an application case of the developed system is discussed. Conclusions and final remarks are drawn in Section 7.

2 | PRINCIPLE OF THE IMPROVED DOUBLE-SIDED PD DETECTION AND LOCATION METHOD

2.1 | The classical double-sided location method

When a PD source occurs in the underground cable, high-frequency pulses generated by the PD source can propagate in two directions and to the cable ends, as shown in Figure 1. PD detectors deployed at the double sides of the cable can capture these PD pulses and the PD source location can be estimated by analysing time-of-arrivals (TOAs) of these pulses. The location L_{PD} of the PD source is formulated as

$$L_{PD} = \frac{L_{AB} - (t_B + \Delta t_{SYN} - t_A) \cdot v}{2}, \quad (1)$$

where L_{AB} is the cable length, t_A and t_B are the TOAs of the two pulses originating from the same PD activity and are

17518695, 2023, 11, Downloaded from https://ietresearch.onlinelibrary.wiley.com/doi/10.1049/gtd2.12834 by Politecnico Di Torino Sist. Bibl Del Polit Di Torino, Wiley Online Library on [16/06/2023]. See the Terms and Conditions (https://onlinelibrary.wiley.com/terms-and-conditions) on Wiley Online Library for rules of use; OA articles are governed by the applicable Creative Commons License

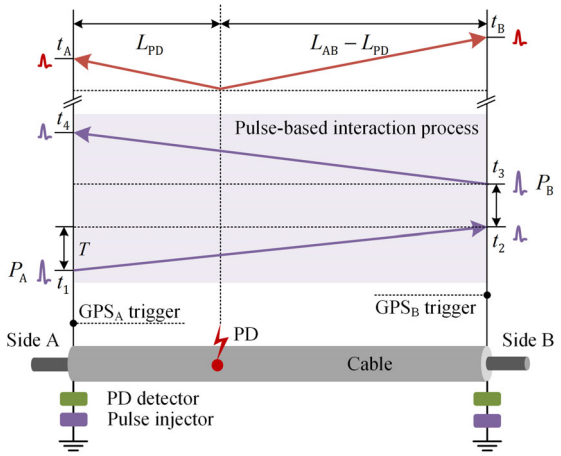

FIGURE 2 The improved double-sided PD location method.

detected by the PD detectors at Sides A and B, respectively, Δt_{SYN} is the synchronisation error between the two PD detectors, which depends on the performance of the GPSs and v is the propagation velocity of the PD pulses, which is unknown and depends on the material and structural properties of the cable [25]. Equation (1) reveals that the PD localisation accuracy strongly depends on the synchronisation error Δt_{SYN}, the estimated propagation velocity v and the estimated TOAs t_A and t_B.

2.2 | The improved double-sided location method

The synchronisation error Δt_{SYN} caused by the double-sided GPSs is inevitable and always randomly fluctuates, depending on the surrounding environment and weather, so we inserted a pulse-based double-sided interaction process into the classical PD location method to eliminate Δt_{SYN} (by simultaneously estimating the propagation velocity v), as shown in Figure 2. The improved PD location method is divided into three subprocesses: (i) GPS triggering, (ii) pulse-based double-sided interaction and (iii) PD localisation. They are described as follows:

Firstly, the two PD detectors are triggered by their respective GPS to collect data. The total length of the data is sampled in one complete power frequency cycle (i.e. 20 ms) to cover enough PD pulses. The collected data in Sides A and B are defined as $u_A(t)$ and $u_B(t)$, respectively.

Secondly, the pulse-based double-sided interaction process is activated after triggering GPS within a short time window (e.g. 100 μs). A three-step procedure is described as follows (see Figure 2) to better explain the process:

Step 1) A pulse P_A generated by the pulse injector is injected into the cable at Side A at the time t_1. The pulse P_A propagates along the cable and arrives at Side B at the time t_2.

Step 2) The other pulse P_B is injected into the cable at Side B at the time t_3 ($t_3 > t_2$) after a time delay. The pulse P_B propagates along the cable and arrives at Side A at the time t_4. The propagation time of the injected pulses from Side A to Side B can be calculated as follows:

$$T = \frac{(t_4 - t_1) - (t_3 - t_2)}{2}. \tag{2}$$

The propagation velocity of the injected pulses in the cable can be estimated by

$$v = \frac{L_{AB}}{T}. \tag{3}$$

Step 3) The absolute time zero of the data sequence $u_A(t)$ is defined as t_1, whereas that of the data sequence $u_B(t)$ is defined as $(t_2 - T)$. The synchronisation error Δt_{SYN} in Equation (1) can be thus estimated as

$$\Delta t_{SYN} = t_1 - t_2 + T. \tag{4}$$

Finally, after the pulse-based double-sided interaction process, the two detectors continue to collect PD data until the sampling time reaches 20 ms. Incorporating Equations (1), (2), (3) and (4), the PD location L_{PD} can be rewritten as

$$L_{PD} = \frac{L_{AB} \cdot [(t_A - t_B) - (t_1 - t_2)]}{(t_4 - t_1) - (t_3 - t_2)}. \tag{5}$$

In contrast to Equation (1), Equation (5) eliminates the synchronisation error and the need for the exact propagation velocity.

In the above process, the amplitudes of the injected pulses should be significantly larger (e.g. several V) than those of PD pulses (i.e. weak signals with several, tens or at most hundreds of mV) in order to ease its identification. The solution in this paper is to use a high-amplitude pulse generator, which will be described in Section 4.1. Moreover, elimination of the influence of PD pulses or impulse noises can also be achieved via repeatedly activating the pulse-based double-sided interaction process since PD pulses or impulse noises always occur randomly, whilst the injected pulses always occur at the set time.

3 | PRINCIPLES OF THE IMPROVED TIME-OF-ARRIVAL DIFFERENCE ESTIMATION METHOD

According to Equation (5), the PD localisation accuracy depends on the estimation accuracy of TOAs of the injected pulses and PD pulses. Since the injected pulses are controllable and their amplitude and rising time can be deliberately set to be high and fast, respectively, the TOAs of the injected pulses t_1, t_2, t_3 and t_4 can be easily determined via the simple threshold method. In contrast, determining the TOAs of the PD pulses is challenging as their amplitudes are always low, causing them to be susceptible to background noise

17518695, 2023, 11, Downloaded from https://ietresearch.onlinelibrary.wiley.com/doi/10.1049/gtd2.12834 by Politecnico Di Torino Sist. Bibl Del Polit Di Torino, Wiley Online Library on [16/06/2023]. See the Terms and Conditions (https://onlinelibrary.wiley.com/terms-and-conditions) on Wiley Online Library for rules of use; OA articles are governed by the applicable Creative Commons License

interferences [26]. In this section, a windowed phase difference method is developed to robustly estimate the TOA difference of the PD pulses (i.e. the sub-equation $\Delta t = (t_A - t_B)$ in Equation (5)) to reduce the influence of the noise interferences. In order to better explain the method, the classical phase difference method is first reviewed and the developed method is subsequently described.

3.1 | Classical phase difference method

Let us consider two noisy sub-signals $x_A(t)$ and $x_B(t)$, obtained by sliding a time window with the length T_{win} on $u_A(t)$ and $u_B(t)$, respectively. T_{win} can be conveniently chosen to be two to three times the propagation time T of the PD pulses travelling in the entire cable. In the time window, $x_A(t)$ and $x_B(t)$ contain a PD pulse, respectively, and the pulses in $x_A(t)$ and $x_B(t)$ originate from the same PD activity. Examples of $x_A(t)$ and $x_B(t)$ can be found in the laboratory and field experiences in Section 5.

While PD pulses between $x_A(t)$ and $x_B(t)$ are related, since noises between $x_A(t)$ and $x_B(t)$ are generally unrelated, correlation analysis between $x_A(t)$ and $x_B(t)$ can reduce the influence of the noises on determining their TOA difference [27]. The phase difference method is a representative correlation analysis approach to estimate the TOA difference between two related signals [21, 28]. It provides the TOA difference estimation only based on the cross-power spectrum phase, that is, the phase of the frequency domain representation of the cross-correlation between the two signals $x_A(t)$ and $x_B(t)$. The phase difference method is completed in the following three steps.

Step 1) Cross-power spectrum $\Psi(\omega)$ of the two signals $x_A(t)$ and $x_B(t)$ is calculated as

$$\Psi(\omega) = \frac{X_A(\omega) \cdot X_B^*(\omega)}{\left| X_A(\omega) \cdot X_B^*(\omega) \right|}, \tag{6}$$

where $X_A(\omega) \in \mathbb{C}$ is the Fourier transform of $x_A(t)$ and $X_B^*(\omega) \in \mathbb{C}$ is the complex conjugation of the Fourier transform of $x_B(t)$. The $\Psi(\omega)$ modulus (i.e. $|\Psi(\omega)|$) is identically equal to 1 and the phase of $\Psi(\omega)$ (i.e. $\angle\Psi(\omega)$) is equal to the phase difference between $X_A(\omega)$ and $X_B(\omega)$.

Step 2) Generalised cross-correlation $R(\tau)$ of the two signals $x_A(t)$ and $x_B(t)$ is defined as the inverse Fourier transform of $\Psi(\omega)$, that is

$$R(\tau) = \frac{1}{2\pi} \int_{-\pi}^{\pi} \Psi(\omega) \cdot e^{j\omega\tau} \, d\omega. \tag{7}$$

Step 3) The TOA difference Δt between the pulses in $x_A(t)$ and $x_B(t)$ is estimated by searching for the maximum absolute value of $R(\tau)$, as follows [28]:

$$\Delta t = \arg \max_{\tau} |R(\tau)|, \tag{8}$$

where Δt is always positive, because Equation (8) assumes that the PD pulse in $x_A(t)$ is later than that in $x_B(t)$ (i.e. $t_A > t_B$). If the PD pulse in $x_A(t)$ is earlier than that in $x_B(t)$, Δt should be redefined as $(\Delta t - T_{win})$. The chronological order of the two PD pulses in $x_A(t)$ and $x_B(t)$, respectively, can be conveniently determined by comparing the times corresponding to their peaks.

3.2 | The improved windowed phase difference method

According to Equation (7), it can be observed that $R(\tau)$ uses all the frequency components in $\Psi(\omega)$. This is a good strategy and can make the result robust if the target signals have a wide frequency spectrum distribution. However, in practice, the main energy of the frequency spectrum of PD signals measured in cables is always limited in a relatively narrow frequency sub-band (e.g. a few MHz), while noises are almost distributed in the entire frequency pass-band (e.g. tens or hundreds of MHz) [23]. Therefore, selecting the PD-associated frequency sub-band in $\Psi(\omega)$ to calculate $R(\tau)$ can improve the robustness of the TOA difference estimation. Since the exact central value of the frequency sub-band of PD pulses is unknown in field measurement, depending on the material, size and location of the PD source [29], we apply a sliding frequency-domain window on $\Psi(\omega)$. Equation (7) can be rewritten as

$$r(\tau, l) = \frac{1}{2\pi} \int_{-\pi}^{\pi} \Psi(\omega) \cdot G(|\omega| - \omega_l) \cdot e^{j\omega\tau} \, d\omega, \tag{9}$$

where ω_l is the frequency offset corresponding to sub-band l, $G(\cdot)$ is a symmetric Gaussian frequency-domain window, centered at $\omega = 0$ with frequency support $[-B_G, B_G]$. In principle, the B_G value depends on the frequency components of the measured PD signal. Since the main energy of the frequency bandwidth of the PD signals measured in MV cables is always within a few MHz [14, 15, 20, 22], B_G can be conveniently set as a few MHz, for example, 2 MHz, which is used in the subsequent laboratory and field experiments and is validated to be feasible.

A two-dimensional generalised cross-correlation spectrum $r(\tau, l)$ can be obtained by sweeping the cross-power spectrum $\Psi(\omega)$ over the frequency sub-bands:

$$\omega_l = l \ldots H_G, \; l = 0, 1, \ldots, L - 1, \tag{10}$$

where H_G is the frequency hop and L is the number of sub-bands and can be chosen to cover those frequencies up to the Nyquist limit of $L = \lfloor (\pi - B_G + H_G)/H_G \rfloor$. In principle,

17518695, 2023, 11, Downloaded from https://ietresearch.onlinelibrary.wiley.com/doi/10.1049/gtd2.12834 by Politecnico Di Torino Sist. Bibl Del Polit Di Torino, Wiley Online Library on [16/06/2023]. See the Terms and Conditions (https://onlinelibrary.wiley.com/terms-and-conditions) on Wiley Online Library for rules of use; OA articles are governed by the applicable Creative Commons License

the smaller the H_G value, the higher the resolution of $r(\tau, l)$ is. On the other hand, too small H_G can lead to additional computational overhead. Therefore, the H_G is recommended to be empirically set as about one-fifth of B_G.

To eliminate the influence of noises, we need to first identify the sub-band l_0 containing most of the PD signal components and then estimate Δt by searching for the maximum absolute value of $r(\tau, l_0)$ as formulated in Equation (8). Since the sub-band with PD signal can produce a larger maximum absolute value of $r(\tau, l_0)$ than that of noises, the above two steps can be completed simultaneously by searching the maximum absolute value of $r(\tau, l)$, which is formulated as

$$\Delta t = arg \max_{\tau} |r(\tau, l)|. \quad (11)$$

Similar to Equation (8), Δt in Equation (11) should be redefined as $(\Delta t - T_{\text{win}})$ if the PD pulse in $x_A(t)$ is earlier than that in $x_B(t)$.

Moreover, when the proposed method is used for the farm wind cables, some possible concerns are specifically clarified as follows.

First, it is important to point out that since the physical structures and electrical parameters of the terminals at both ends of a farm wind inter-array cable are always symmetrical [30], the waveforms between PD signals collected by the double-sided PD detectors are similar, despite the difference in their magnitudes (more details can be found in measured PD signals in Section 6). This is the premise of the phase difference method effectiveness, based on the correlation between the PD signals.

Second, the high-frequency attenuation and dispersion nature of the cables can cause the PD waveform to become 'shorter' and 'fatter' [31]. If the PD source does not locate in the cable middle (i.e. $L_{AB}/2$), the waveforms between the PD signals detected at both ends of the cable can differ, more or less. Nevertheless, in [22], it has been proven that the influence of the attenuation and dispersion characteristics on the phase difference method accuracy is negligible.

In addition, since the running cable is connected to other cables, some reflections caused by the impedance discontinuities (i.e. other cable terminals) can be detected after the PD signal. The reflections magnitude is significantly lower than that of the PD signal due to the high-frequency attenuation nature of the cables [25]. In [20], it has been proven that the low-amplitude reflections hardly reduced the phase difference method accuracy.

4 | IMPLEMENTATION OF THE PORTABLE PD DETECTION AND LOCATION SYSTEM

The developed system consists of a server and two PD testing units, as shown in Figure 3. Each testing unit, which includes a hybrid sensor and an analyser, is deployed at each side of the cable. The weight of each testing unit is less than 10 kg; thus, it is easy to carry and install. The hybrid sensor is installed on the earth wire of the cable. During a measurement, the server sends orders to start the testing units and receives the collected PD data via a 4G/5G communication network. A comprehensive analysis of the PD data from the testing units is completed on the server. More key details of the hybrid sensor and analyser are described in the following sub-sections.

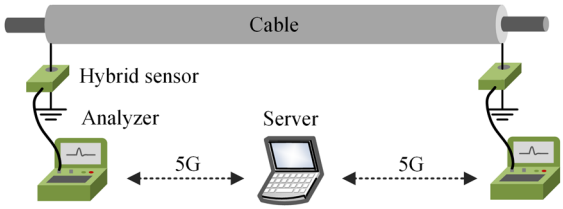

FIGURE 3 Schematic of the portable double-sided PD detection and location system.

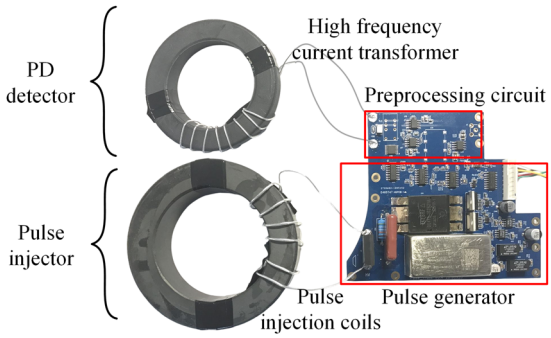

FIGURE 4 Components of the hybrid sensor.

4.1 | Hybrid sensor

The hybrid sensor consisted of a PD detector and a pulse injector, as shown in Figure 4. The PD detector consists of a high-frequency current transformer and a pre-processing circuit and the pulse injector consists of pulse injection coils and a simplified pulse generator. Implementation of the components in the hybrid sensor is described as follows.

A high-frequency current transformer is used as the sensor in the PD detector because of its high sensitivity, wide frequency band and non-invasive placement [32]. The pre-processing circuit consists of a transient overvoltage protection module to protect the sequent circuit from the injected high-amplitude pulses and an instrumentation amplifier with a gain of 0 dB and pass-band frequency from 0.1 to 20 MHz. The sensitivity and pass-band frequency of the whole PD detector were measured as 5.6 mV/mA and 0.18–20.3 MHz, respectively.

The pulse injection coils have a manganese zinc ferrite core with high magnetic permeability of 3000 to increase the coupling efficiency of the injected pulse. The equivalent circuit of the pulse generator is shown in Figure 5. The working procedure of the pulse generator is briefly described as follows. First, the metal-oxide-semiconductor field-effect transistor G (DE475-102N21A, IXYS) is opened and the 1,000-V DC

17518695, 2023, 11, Downloaded from https://ietresearch.onlinelibrary.wiley.com/doi/10.1049/gtd2.12834 by Politecnico Di Torino Sist. Bibl Del Polit Di Torino, Wiley Online Library on [16/06/2023]. See the Terms and Conditions (https://onlinelibrary.wiley.com/terms-and-conditions) on Wiley Online Library for rules of use; OA articles are governed by the applicable Creative Commons License

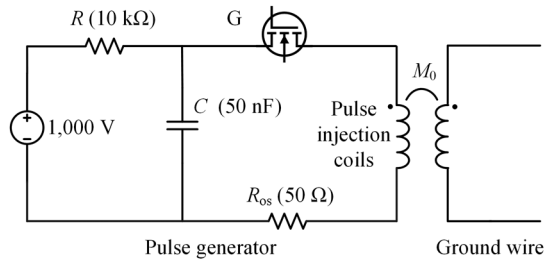

FIGURE 5 Equivalent circuit of the pulse generator and pulse injection coils.

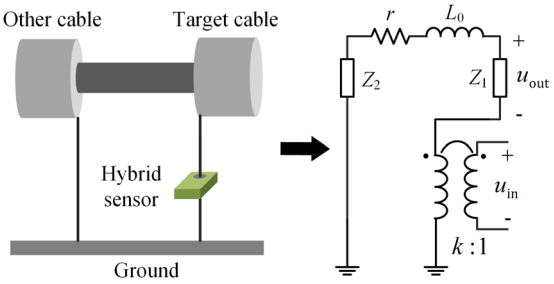

FIGURE 6 Equivalent circuit of the pulse injection process in a running cable.

supply charges the capacitor C with the current-limiting resistance R. Second when a pulse needs to be injected, G is closed for a short while (e.g. 400 ns) and then opened again. As a result, a high-amplitude pulse is produced on the coils and partly coupled to the earth wire of the cable via the mutual inductance M_0. The role of the damping resistance R_{os} in series with the pulse injection coils is to suppress the high-frequency oscillation of the injected pulse. Moreover, it is important to point out that the additional pulse injector hardly increases the cost of the system since its total cost is only 100 USD, which is significantly less than that of the high-speed acquisition and processing system in the analyzer (e.g. with the cost of about 2500 USD).

The pulse coupled to the earth wire can further be coupled to the target cable, as shown in Figure 6. The voltage $u_{out}(\omega)$ of the pulse coupled to the target cable can be calculated in the frequency-domain as

$$u_{out}(\omega) = k.\frac{Z_1}{Z_1 + Z_2 + r + j\omega L_0}.u_{in}(\omega), \tag{12}$$

where $u_{in}(\omega)$ is the voltage of the generated pulse on the pulse injection coils, k is the coupling ratio of the pulse injection coils (e.g. 0.1), Z_1 is the impedance of the target cable, Z_2 is the impedance of the power equipment connected to the target cable, that is, one or more cables, and r and L_0 are, respectively, the equivalent resistance and inductance of the loop that consists of the ground, the earth wires and the conductor connecting the two cables. Since the main energy of the frequency spectrum of the injected pulse is concentrated in the range of a few MHz, $(r + j\omega L_0)$ is much smaller than $(Z_1 + Z_2)$. Therefore, Equation (12) can be simplified as

$$u_{out}(\omega) \approx k \cdot \frac{Z_1}{Z_1 + Z_2} \cdot u_{in}(\omega). \tag{13}$$

It reveals that the generated pulse on the injection coils can be proportionally injected into the cable.

4.2 | Analyser

The analyser consists of four components: a central processing module, a 5G communication module (5G RG200U-CN, QUECTEL), a commercial GPS module (UM220-III, UNICORECOMM) and an improved data collection module. The data collection module is equipped with a single-channel analogue-to-digital converter (ADC) with a resolution of 12-bit and a sampling rate of 125 MS/s. The time base error between the two ADCs of the double-sided analysers is inevitable and mainly depended on the frequency accuracy of their crystal oscillators. The error can gradually accumulate as sampling time increases, leading to non-negligible PD location errors. Thus, the conventional voltage-controlled crystal oscillator in the commercial ADC, which has a frequency error of several ppm, is specifically replaced by the oven-controlled crystal oscillator (AOCJY7TQ, ABRACON) for such application of double-sided PD localisation. AOCJY7TQ has less than 0.05 ppm frequency error in the temperature range from −40°C to 70°C. In other words, the time base error between the two improved data collection modules is less than 1 ns while the sampling time was up to 20 ms.

5 | LABORATORY VALIDATION EXPERIMENT

5.1 | Layout of the testing platform

A testing platform with a 353-m 10-kV cross-linked polyethylene cable was built in the laboratory to validate the effectiveness and feasibility of the proposed methods and developed system, as shown in Figure 7. Since a running wind farm cable is always connected to other cables in practice, two 30 Ω resistors were connected with the double sides of the cable to simulate the impedances of these outer cables. Two testing units were deployed at the double sides of the cable and hybrid sensors were mounted on the earth wires of the cable. A laptop (the server) was used to control the two testing units and collect and analyse the measured data. A programmable PD simulator was used to simulate a PD source and was mounted on the cable 161 m from Side A. The principle of injecting the simulated PD pulses via the PD simulator is similar to that of the developed pulse injector in the hybrid sensor. The PD simulator can produce a series of pulses with waveforms similar to those of real PD pulses in cables, that is, the most representative double exponential attenuation pulses [33] (More waveform details of the simulated PD pulses can be found in Section 5.3).

17518695, 2023, 11, Downloaded from https://ietresearch.onlinelibrary.wiley.com/doi/10.1049/gtd2.12834 by Politecnico Di Torino Sist. Bibl Del Polit Di Torino, Wiley Online Library on [16/06/2023]. See the Terms and Conditions (https://onlinelibrary.wiley.com/terms-and-conditions) on Wiley Online Library for rules of use; OA articles are governed by the applicable Creative Commons License

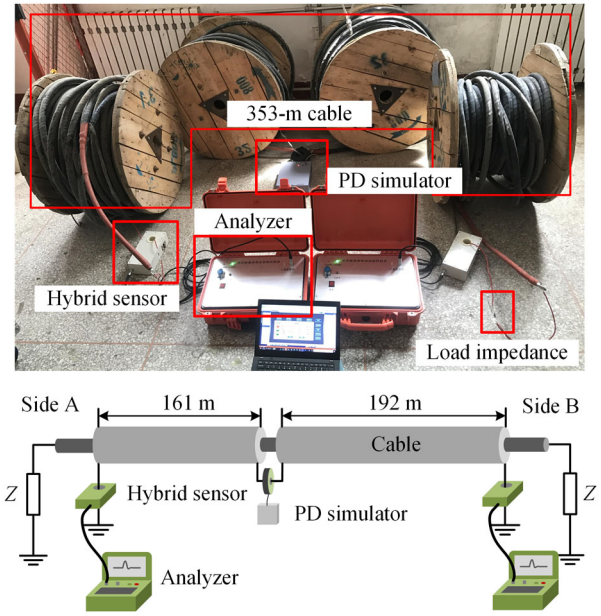

FIGURE 7 Layout of the testing platform.

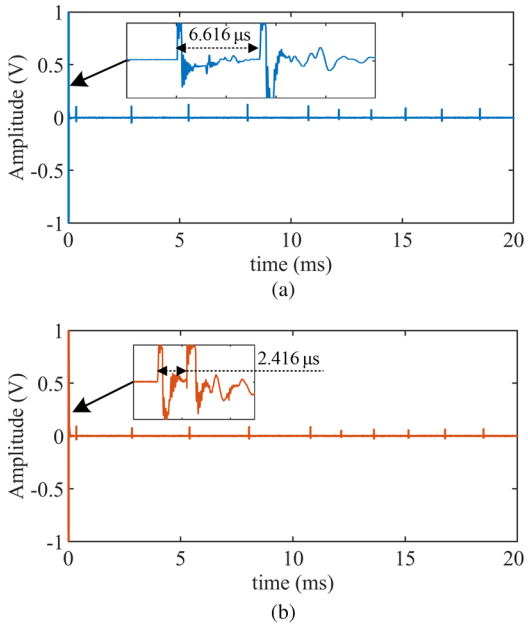

FIGURE 8 Waveforms of the collected signals (The zoomed-in insets display the waveform details of the injected pulses); (a) at Side A and (b) at Side B.

5.2 | PD location results

The amplitude of the pulses produced by the simulator was programmed to vary from approximately 0.2 to 0.4 V. The two testing units were triggered by their respective GPSs to collect data. The signals recorded by the two testing units are shown in Figure 8. The injected pulses are located at the start of the collected signals, and their TOAs are calculated as $t_1 = 5.008\ \mu$s, $t_2 = 7.300\ \mu$s, $t_3 = 9.716\ \mu$s, $t_4 = 11.624\ \mu$s. Calculations of the propagation time of the injected pulses via Equation (2) reveal that the pulse was travelling from Side A to Side B in 2.100 μs, indicating the pulse propagation velocity of 168.1 m/μs. The synchronisation error of the GPSs is calculated as 0.192 μs via Equation (4). Taking the first PD pulse after the inject pulses as an example, the TOA difference (i.e. $(t_A - t_B)$) is calculated as $-0.380\ \mu$s. Finally, the PD location is calculated as 161.0 m via Equation (5).

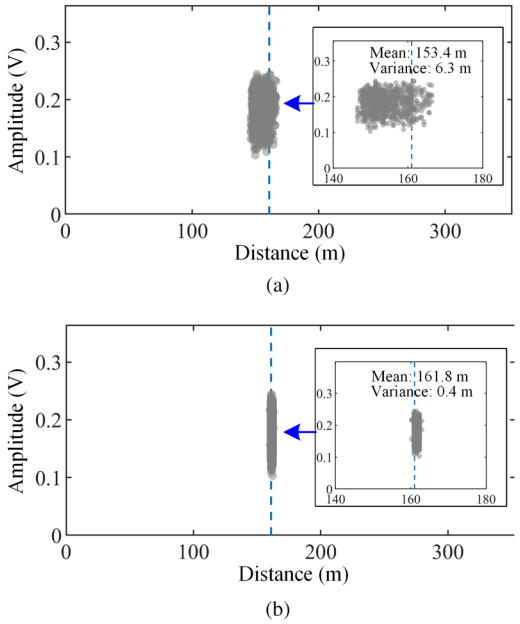

FIGURE 9 PD location maps (blue dotted lines denote the actual location of the PD simulator and grey dots denote partial discharge events); (a) the classical method and (b) the proposed method.

The above measurement was repeated 150 times. With all the recorded data, the PD location of each simulated PD event was calculated and is shown in Figure 9. Figure 9a collects the PD location map obtained by the classical double-sided PD location method, using the trigger time of the GPS as the absolute time zero. It can be observed that the mean of the PD events deviated significantly from the actual value and their variance is also large. Moreover, the mean deviation and variance are expected to be larger in field measurement due to possible larger synchronisation errors of GPSs caused by the more complex and diverse environment and weather, as well as without providing the pulse propagation velocity. Figure 9b collects the PD location map obtained by the proposed PD location method, using the injected pulses to redefine the absolute time zero in each measurement. It can be observed that the mean of the PD events is close to the actual value and their variance is very small.

In conclusion, the added pulse-based interaction process of the proposed method can significantly improve PD location accuracy. Nevertheless, it is important to point out that the GPS triggers are still essential in field measurement because they can ensure that the double-sided testing units are reliably triggered even in a high-level noise environment, which is the premise for the pulse-based interaction process to function normally.

17518695, 2023, 11, Downloaded from https://ietresearch.onlinelibrary.wiley.com/doi/10.1049/gtd2.12834 by Politecnico Di Torino Sist. Bibl Del Polit Di Torino, Wiley Online Library on [16/06/2023]. See the Terms and Conditions (https://onlinelibrary.wiley.com/terms-and-conditions) on Wiley Online Library for rules of use; OA articles are governed by the applicable Creative Commons License

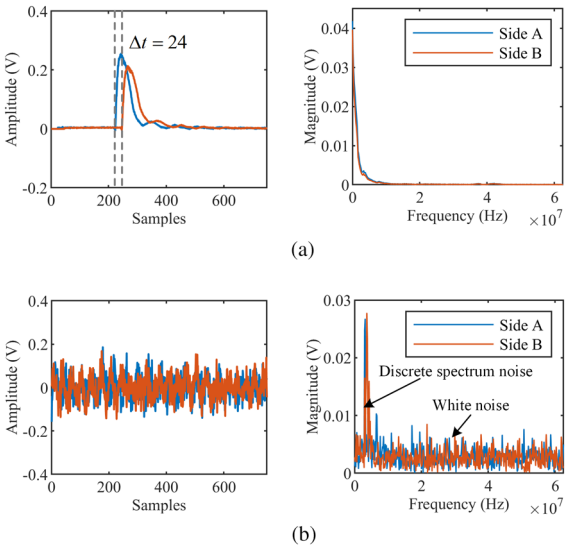

FIGURE 10 Time-domain and frequency-domain waveforms of the PD pulses and noises collected by the developed system. (a) Simulated noiseless PD signals measured in the laboratory cable and (b) the noises measured in a real 2032-m 35-kV cable in an on-shore wind farm.

5.3 | Time-of-arrival difference estimate results

In this sub-section, the proposed TOA difference estimate method is applied to synthetic noisy PD signals, which are fully controllable and can be used to validate and stress the method in extreme conditions (e.g. with a very large impact of noise). Simultaneously, the proposed method is compared with the state-of-the-art alternatives, the energy criterion method [20] and the phase difference method [22].

The synthetic noisy PD signals were obtained by proportionally adding noises on noiseless PD signals. The noiseless PD signals are the simulated pulses measured by the developed system in the laboratory cable, as shown in Figure 10a. The onsets of the two noiseless pulses can be visually identified and their TOA difference is calculated as 24 sampling points. As shown in Figure 10b, the noises were measured by the developed system in a real 2032-m 35-kV cable in an on-shore wind farm. It can be observed that the noises contain both representative white noise and discrete spectrum noise. In addition, the centre frequency of the discrete spectrum noise is close to that of the PD pulses. Thus, the noises can be used to simulate the worst noise case in field measurement.

The waveforms of the synthetic noisy PD signals, their cross-power spectrum phase curve and the TOA difference estimate results are shown in Figure 11. Three possible situations are considered: (i) Case I: no noise, (ii) Case II: low-level noise, (iii) Case III: high-level noise. According to the recommended parameter selection of the proposed method in Section 3.2, the value of frequency support B_G is set as 2 MHz (i.e. 12 sampling points when the sampling frequency is 125 MHz and the total number of sampling points is 750). The value of the frequency hop H_G turns out to be 0.4 MHz (i.e. 2 sampling points). In Case I, no noise is added to the synthetic PD signals and thus, their cross-power spectrum phase curve (i.e. $\angle\Psi(\omega)$ is almost perfect to be used in the phase difference method for TOA difference estimation, as shown in the first row and the first column in Figure 11. Because the TOA difference between the various frequency components of the two signals is a constant, the phase difference between the two PD signals increases as the frequency increases, causing the phase curve to be a sawtooth wave. The TOA difference estimation results reveal that the energy criterion, phase difference and the proposed methods all perform perfectly, as shown in the last three columns of the first row in Figure 11.

In Case II, low-level noises are added to the synthetic PD signals and the sawtooth wave characteristic of the cross-power spectrum phase curve becomes unclear, as shown in the second row and the first column in Figure 11. Compared with the noiseless signals in Case I, it is quite difficult to visually identify the onsets of the noisy PD signals. Nevertheless, the energy criterion, phase difference and the proposed methods are still effective, as shown in the last three columns of the second row in Figure 11. Moreover, the results reveal that the errors of the energy criterion and phase difference method are slightly larger than that of the proposed method.

In Case III, high-level noises are added to the synthetic PD signals and the sawtooth wave characteristic of the cross-power spectrum phase curve is more unclear, as shown in the last row and first column in Figure 11. The results reveal that the energy criterion and phase difference methods fail to estimate the TOA difference, while the proposed method is still effective, despite having a small error, as shown in the last three columns of the second row in Figure 11.

In conclusion, the proposed TOA difference estimation method performs more robustly than the state-of-the-art energy criterion and phase difference methods in a low signal-to-noise ratio environment, which is actually inevitable in the online PD measurement of wind farm cables.

6 | AN APPLICATION CASE

On-site testing was carried out on a real 485-m 35-kV cross-linked polyethene cable in an on-shore wind farm, as shown in Figure 12. Two testing units were conveniently mounted on the earth wires of the cable. The two testing units collected the noisy PD signals, as shown in Figure 13. The injected pulses are located at the start of the collected signals, and their TOAs are calculated as $t_1 = 5.008\ \mu$s, $t_2 = 7.424\ \mu$s, $t_3 = 10.272\ \mu$s, $t_4 = 32.328\ \mu$s. Calculations of the propagation time of the injected pulses via Equation (2) reveal that the pulse travelled from Side A to Side B in 2.848 μs, which equates to a pulse propagation velocity of 170.3 m/μs. Moreover, the synchronisation error of the GPSs is calculated as 0.432 μs via Equation (4), leading to several tens of meters of PD location error, demonstrating the necessity of the pulse-based interaction process.

In addition, it can be observed in Figure 13 that the signals contain severe noises, including continuous noise interferences and various impulse noise interferences, causing it to be

17518695, 2023, 11, Downloaded from https://ietresearch.onlinelibrary.wiley.com/doi/10.1049/gtd2.12834 by Politecnico Di Torino Sist. Bibl Del Polit Di Torino, Wiley Online Library on [16/06/2023]. See the Terms and Conditions (https://onlinelibrary.wiley.com/terms-and-conditions) on Wiley Online Library for rules of use; OA articles are governed by the applicable Creative Commons License

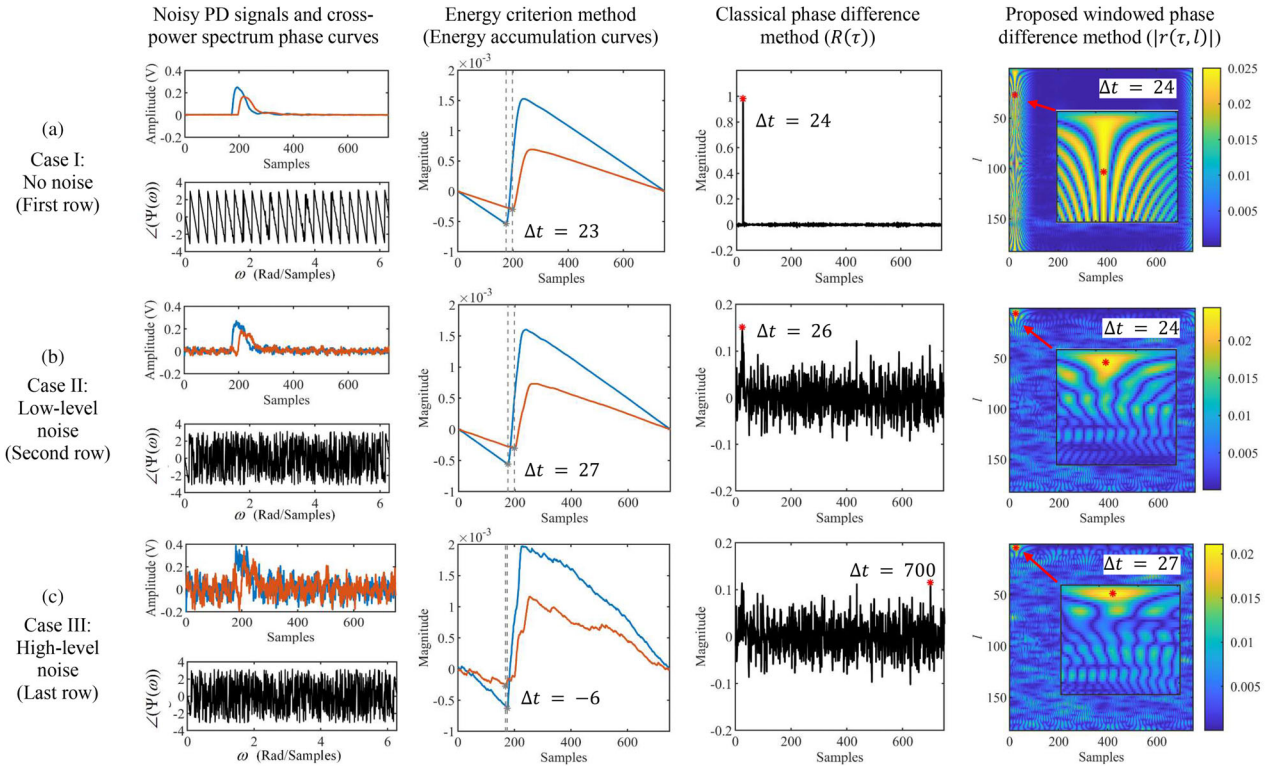

FIGURE 11 Results of the time-of-arrival difference estimation in varying noise levels, by means of the energy criterion, classical phase difference and the proposed windowed phase difference methods. (The grey star marks denote the minimum values of the energy accumulation curves and the red star marks denote the maximum values of generalised cross-correlation $R(\tau)$ or the two-dimensional generalised cross-correlation spectrum $|r(\tau, l)|$). (a) Case I: no noise. (b) Case II: low-level noise. (c) Case III: high-level noise.

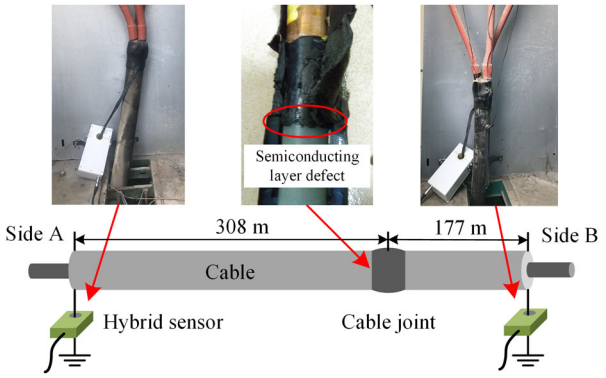

FIGURE 12 Layout of the developed system on a real 485-m 35-kV cable in an on-shore wind farm.

challenging to identify any PD activity. To further interpret the collected signals, their PD location map was calculated via a three-step procedure as follows:

Step 1) A threshold value is defined to identify the pulses in each signal. It is set as 3σ, a statistic value suggested in [34], where σ is the standard deviation of the signal. The threshold values of the signals collected at Side A and Side B are calculated as 0.023 and 0.052 V, respectively. In addition, the window width T_{win} is set as 750 (i.e. 6 μs) to extract pulses, which is wide enough to cover a PD pulse.

Step 2) TOA differences between the pulses of the two signals are calculated via the proposed TOA estimation method, as shown in Figure 14. Similar to laboratory experiments, the parameters B_G and H_G are set as 2 MHz (i.e. 12 sampling points) and 0.4 MHz (i.e. 2 sampling points), respectively.

Step 3) PD locations are further calculated, as shown in Figure 15. It can be observed that there are repeated PD events located at 310.7 m from Side A, where there is a middle joint 308 m from Side A. In addition, it is important to point out that although a few PD pulses can inevitably overlap with the impulse noise, which may lead to errors of a single PD location estimation (like these randomly distributed scattered points in Figure 15), the accuracy of the final PD location estimation is hardly reduced by these spurious points since it is identified via statistically averaging the location values of the concentrated points (like the cluster of the points in the middle of Figure 15)

After 5 days of this testing, the staff replaced and dissected the joint, as shown in the middle of Figure 12. Visible damage to the semiconductor layer due to improper manual manipulation was observed. Then we ran a second PD test on the cable.

17518695, 2023, 11, Downloaded from https://ietresearch.onlinelibrary.wiley.com/doi/10.1049/gtd2.12834 by Politecnico Di Torino Sist. Bibl Del Polit Di Torino, Wiley Online Library on [16/06/2023]. See the Terms and Conditions (https://onlinelibrary.wiley.com/terms-and-conditions) on Wiley Online Library for rules of use; OA articles are governed by the applicable Creative Commons License

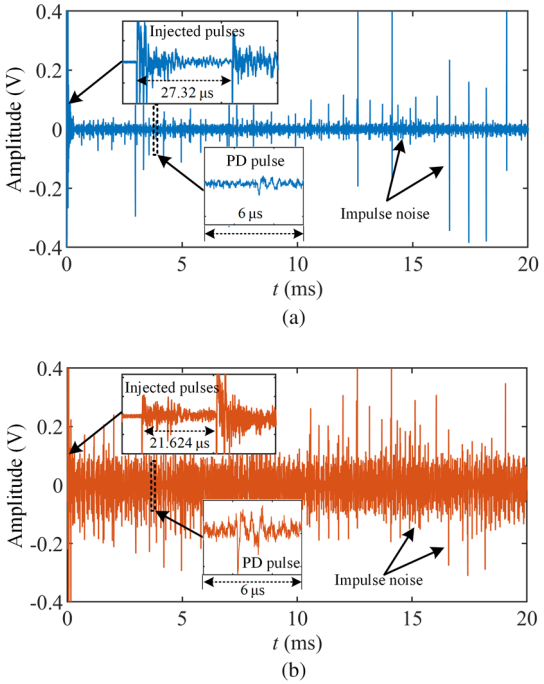

FIGURE 13 Waveforms of the collected noisy PD signals. (The zoomed-in insets display the waveform details of the injected pulses, PD pulse and impulse noise interferences); (a) at Side A and (b) at Side B.

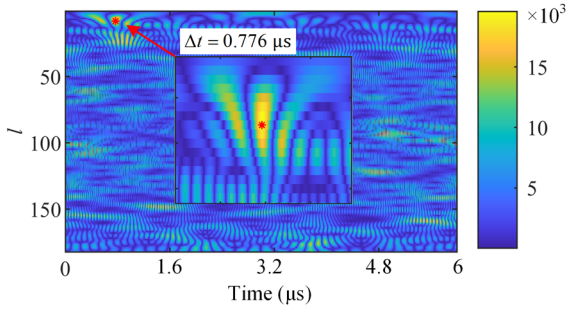

FIGURE 14 Estimation results of the time-of-arrival difference between the two PD pulses in the zoomed-in inset in Figure 13 after eliminating the synchronization error of the GPSs. (the red star mark denotes the maximum value of the two-dimensional generalised cross-correlation spectrum $|r(\tau, l)|$).

No PD event was found, thereby confirming that the damage of the semiconductor layer was the cause of the PD events and demonstrating the effectiveness and accuracy of the proposed methods and system.

Moreover, Figure 15 also shows that the other two clusters of repeated events locate at the double sides of the PD location map and are similar to the cluster of the PD events. So, it can be inferred that the two clusters were caused by the impulse noise interferences that may originate from the other power equipment connected to the cable, for example, the corona discharges from overhead lines or the switching noise from wind turbine gearboxes [35]. It can be observed that the PD pulses and the impulse noise interferences, which are mixed in the time domain (see Figure 13), can be automatically separated in the PD location map. This reveals that the PD location map can assist in eliminating the influence of impulse noise interferences

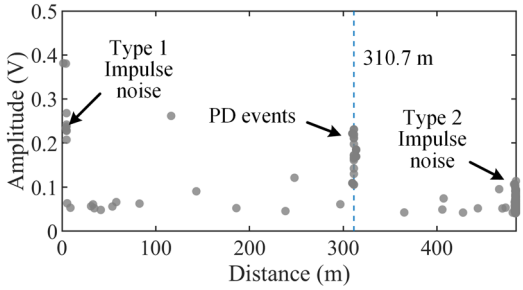

FIGURE 15 PD location map.

TABLE 1 Comparison of the developed system and the commercial off-line PD measurement systems

Feature	35-kV series resonance PD measurement system [36]	40-kV oscillating wave PD measurement system [37]	Developed system
Weight	1100 kg	80 kg	20 kg
Cost	≈200,000$	≈100,000$	≈8,000$
Testing time	> 4 h	≈ 3 h	≈ 20 min
Manpower	>10	5	3

on online PD measurement, demonstrating the added benefit of the double-sided PD detection and location method.

Finally, it is essential to mention that the entire testing process—including the installation of testing units, signal collection and data analysis—was completed within 20 min, requiring only three technicians (two for PD measurement system installation and one for data analysis). Table 1 lists a detailed comparison of the developed system and the widely used off-line PD measurement systems (i.e. series resonance PD measurement system [36] and oscillating wave PD measurement system [37]) on weight, cost, time for one testing, and required manpower. It can be observed that compared with the commercial off-line PD measurement systems, which require a heavy high voltage generator, dozens of technicians, and several hours for a PD measurement, the developed system is more portable, cost-effective, time-saving and manpower-saving, thus allowing more high-efficiency PD measurement of numerous and widely distributed inter-array cables in wind farms.

7 | CONCLUSION

In this paper, a portable PD detection and location system is developed to online assess the insulation condition of wind farm inter-array cables. An improved double-sided travelling wave method achieves PD detection and localisation in this system. The proposed solution offers three important technical benefits: (1) The hybrid synchronisation approach is developed via the joint application of Global Position Systems and the pulse-based interaction process. The synchronisation approach not only can eliminate the inherent random errors of the GPSs

17518695, 2023, 11, Downloaded from https://ietresearch.onlinelibrary.wiley.com/doi/10.1049/gtd2.12834 by Politecnico Di Torino Sist. Bibl Del Polit Di Torino, Wiley Online Library on [16/06/2023]. See the Terms and Conditions (https://onlinelibrary.wiley.com/terms-and-conditions) on Wiley Online Library for rules of use; OA articles are governed by the applicable Creative Commons License

but also estimate the pulse propagation velocity of the cable, thus improving on-site PD localisation; (2) An windowed phase difference method is developed to robustly estimate the time-of-arrival difference between the noisy PD pulses collected by the detectors in low signal-to-noise ratio environment, guaranteeing accurate and reliable PD location identification in the field; (3) The PD location map can automatically separate PD pulses from impulse noise interferences, enabling the easy elimination of their influence. Both laboratory experiments on a 353-m 10-kV cable and an application case on a real 485-m 35 kV cable in an on-shore wind farm validated the effectiveness and accuracy of the proposed methods and system.

Moreover, it is important to remark that the proposed portable online PD detection and location technique turns out to be more cost-effective, time-saving and manpower-saving than the classical offline PD measurement techniques, and can support more high-efficiency condition-based maintenance of the numerous wind farm cables.

Future works will investigate a possible application or improvement of the proposed TOA estimation method for more complex cases, for example, with a big difference between the double-sided PD pulses caused by asymmetric cable terminations or with high-amplitude reflections behind the PD pulses caused by nearby impedance discontinuous points.

AUTHOR CONTRIBUTIONS

Hongjie Li, and Yuan Yan developed the PD location method; Trinchero, Riccardo, Yuan Yan, and Stievano, Igor Simone developed the TOA estimate algorithm. Yuan Yan, Kun zhao, and Yinsong Zhao conceived and designed the experiments; Yinsong Zhao performed the experiments; Yuan Yan wrote the paper. All authors have read and approved the final manuscript.

ACKNOWLEDGEMENTS

The authors would like to thank the China Scholarship Council for the support and Longyuan (Beijing) Wind Power Engineering Technology Co., Ltd for providing test sites.

CONFLICT OF INTEREST STATEMENT

The authors declare no conflict of interest.

DATA AVAILABILITY STATEMENT

The data that support the findings of this study are available from the corresponding author upon reasonable request.

REFERENCES

1. Gulski, E., Anders, G.J., Jongen, R.A., Parciak, J., Siemiński, J., Piesowicz, E., Paszkiewicz, S., Irska, I.: Discussion of electrical and thermal aspects of offshore wind farms' power cables reliability. Renewable Sustainable Energy Rev. 151, 111580 (2021)
2. Wilson, R.: Best practice guideline for the complete condition monitoring (CM) of offshore wind farm (OWF) cable networks. In: 9th International Conference on Insulated Power Cables. IEEE, Piscataway (2015)
3. Wester, F.J., Gulski, E., Smit, J.J.: Condition based maintenance of MV power cable systems on the basis of advanced PD diagnostics. In: 16th International Conference and Exhibition on Electricity Distribution, Part 1: Contributions. CIRED, vol. 482(1), p. 5. IET, Stevenage, UK (2001)
4. Montanari, G.C., Hebner, R., Seri, P., Ghosh, R.: Self-assessment of health conditions of electrical assets and grid components: A contribution to smart grids. IEEE Trans. Smart Grid. 12(2), 1206–1214 (2021)
5. Mohamed, F.P.; Siew, W.H., Soraghan, J.J., Strachan, S.M., McWilliam, J.: Remote monitoring of partial discharge data from insulated power cables. IET Sci. Meas. Technol. 8(5), 319–326 (2014)
6. Gouda, O.E., ElFarskoury, A.A., Elsinnary, A.R., Farag, A.A.: Investigating the effect of cavity size within medium-voltage power cable on partial discharge behaviour. IET Gener. Transm. Distrib. 12(5), 1190–1197 (2018)
7. Mashikian, M.S., Szarkowski, A.: Medium voltage cable defects revealed by off-line partial discharge testing at power frequency. IEEE Electr. Insul. Mag. 22(4), 24–32 (2006)
8. Gulski, E., Jongen, R., Rakowska, A., Siodla, K.: Offshore wind farms on-site submarine cable testing and diagnosis with damped AC. Energies 12(19), 3703 (2019)
9. He, W., Wu, Z., Deng, B., Wang, Q., Xiang, H., Xie, G., Li, H., Lu, Y.: On-site partial discharge detection of power cables using a novel DAC technique supplied by a capacitor bank. IET Gener. Transm. Distrib. 13(23), 5349–5356 (2019)
10. Halvorson, H.L.: Condition assessment of wind farm medium voltage cable joints. Master's thesis, Norwegian University of Science and Technology (2012)
11. Wu, J., Mor, A.R., Smit, J.J.: The effects of superimposed impulse transients on partial discharge in XLPE cable joint. Int. J. Electr. Power Energy Syst. 110, 497–509 (2019)
12. Mohamed, F.P., Siew, W.H., Soraghan, J.J., Strachan, S.M., McWilliam, J.: Remote monitoring of partial discharge data from insulated power cables. IET Sci. Meas. Technol. 8(5), 319–326 (2014)
13. Harmsen, D., Lamboo, S., Van Minnen, F., Wagenaars, P.: Accurate online fault location and PD activity location results obtained with SCG–a long-term utility experience. CIRED-Open Access Proc. J. 1, 1–5 (2017)
14. Mor, A.R., Morshuis, P.H.F., Llovera, P., Fuster, V.,Quijano, A.: Localization techniques of partial discharges at cable ends in off-line single-sided partial discharge cable measurements. IEEE Trans. Dielectr. Electr. Insul. 23(1), 428–434 (2016)
15. Mohamed, F.P., Siew, W.H., Soraghan, J.J., Strachan, S.M., McWilliam, J.: Partial discharge location in power cables using a double ended method based on time triggering with GPS. IEEE Trans. Dielectr. Electr. Insul. 20(6), 2212–2221 (2013)
16. Shim, I., Soraghan, J.J., Siew, W.H., McPherson, F., Sludden, K., Gale, P.F.: Locating partial discharge in high voltage (HV) cable networks. In: 1999 Annual Report Conference on Electrical Insulation and Dielectric Phenomena, pp. 210–213. IEEE, Piscataway (1999)
17. Van der Wielen, P.C.J.M., Wouters, P.A.A.F., Veen, J., Van Aartrijk, D.M.: Synchronization of on-line PD detection and localization setups using pulse injection. In: Proceedings of the 7th International Conference on Properties and Applications of Dielectric Materials, vol. 1, pp. 327–330. Institute of Electrical and Electronics Engineers, New York (2003)
18. Van Der Wielen, P.C., Veen, J., Wouters, P.A., Steennis, E.F.: On-line partial discharge detection of MV cables with defect localisation (PDOL) based on two time synchronised sensors. In: CIRED 2005–18th International Conference and Exhibition on Electricity Distribution, pp. 1–5. IET, Stevenage, UK (2005)
19. Pereira, H.M., Marques, M., Pinheiro, M.B., Palhares, R., Raczy, T., Steennis, E.F., Almeida, P.M.: Partial discharge on-line monitoring in MV underground power cables as part of condition based maintenance strategy. In: Proceedings of the 22th International Conference on Electricity Distribution (CIRED). IET, Stevenage, UK (2013)
20. Wagenaars, P., Wouters, P.A.A.F., Van Der Wielen, P.C.J.M., Steennis, E.F.: Accurate estimation of the time-of-arrival of partial discharge pulses in cable systems in service. IEEE Trans. Dielectr. Electr. Insul. 15(4), 1190–1199 (2008)
21. Herold, C., Leibfried, T.: Advanced signal processing and modeling for partial discharge diagnosis on mixed power cable systems. IEEE Trans. Dielectr. Electr. Insul. 20(3), 791–800 (2013)

17518695, 2023, 11, Downloaded from https://ietresearch.onlinelibrary.wiley.com/doi/10.1049/gtd2.12834 by Politecnico Di Torino Sist. Bibl Del Polit Di Torino, Wiley Online Library on [16/06/2023]. See the Terms and Conditions (https://onlinelibrary.wiley.com/terms-and-conditions) on Wiley Online Library for rules of use; OA articles are governed by the applicable Creative Commons License

22. Mardiana, R., Su, C.Q.: Partial discharge location in power cables using a phase difference method. IEEE Trans. Dielectr. Electr. Insul. 17(6), 1738–1746 (2010)
23. Zhang, H., Blackburn, T.R., Phung, B.T., Sen, D.: A novel wavelet transform technique for on-line partial discharge measurements: WT de-noising algorithm. IEEE Trans. Dielectr. Electr. Insul. 14(1), 3–14 (2007)
24. Yan, Y., Trinchero, R., Stievano, I.S., Li, H., Xie, Y.Z.: An automatic tool for partial discharge de-noising via short-time fourier transform and matrix factorization. IEEE Trans. Instrum. Meas. 71, 1–12 (2022)
25. Guo, J.J., Boggs, S.A.: High frequency signal propagation in solid dielectric tape shielded power cables. IEEE Trans. Power Deliv. 26(3), 1793–1802 (2011)
26. Sriram, S., Nitin, S., Prabhu, K.M.M., Bastiaans, M.J.: Signal denoising techniques for partial discharge measurements. IEEE Trans. Dielectr. Electr. Insul. 12(6), 1182–1191 (2005)
27. Benesty, J., Chen, J., Huang, Y.: Time-delay estimation via linear interpolation and cross correlation. IEEE Trans. Speech Audio Process. 12(5), 509–519 (2004)
28. Knapp, C., Carter, G.: The generalized correlation method for estimation of time delay. IEEE Trans. Acoust. Speech Signal Process. 24(4), 320–327 (1976)
29. Khan, Q., Refaat, S.S., Abu-Rub, H., Toliyat, H.A., Olesz, M., Darwish, A.: Characterization of defects inside the cable dielectric with partial discharge modelling. IEEE Trans. Instrum. Meas. 70, 1–11 (2020)
30. Fischetti, M., Leth, J., Bech Borchersen, A.: A Mixed-Integer Linear Programming approach to wind farm layout and inter-array cable routing. In: 2015 American Control Conference (ACC), pp. 5907–5912. IEEE, Piscataway (2015)
31. Mahdipour, M., Akbari, A., Werle, P., Borsi, H.: Partial discharge localization on power cables using on-line transfer function. IEEE Trans. Power Deliv. 34(4), 1490–1498 (2019)
32. Shafiq, M., Kiitam, I., Taklaja, P., Kütt, L., Kauhaniemi, K., Palu, I.: Identification and location of PD defects in medium voltage underground power cables using high frequency current transformer. IEEE Access 7, 103608–103618 (2019)
33. Sheng, B., Zhou, C., Hepburn, D.M., Dong, X., Peers, G., Zhou, W., Tang, Z.: Partial discharge pulse propagation in power cable and partial discharge monitoring system. IEEE Trans. Dielectr. Electr. Insul. 21(3), 948–956 (2014)
34. Zhong, J., Bi, X., Shu, Q., Zhang, D., Li, X.: An improved wavelet spectrum segmentation algorithm based on spectral kurtogram for denoising partial discharge signals. IEEE Trans. Instrum. Meas. 70, 1–8 (2021)
35. Yan, Y., Huo, P., Li, H.: Robust on-line partial discharge measurement of 35-kV cables in wind farms via dual sensors. Energy Rep. 9, 9–17 (2023)
36. Volt, H.: AC resonant test systems for on-site testing and off-line diagnostics of medium voltage cables and electric machines. Available from: https://www.highvolt.de/portaldata/1/Resources/HV/Downloads/8-03-3.pdf. Accessed 17 February 2023
37. Ohv diagnositic. DAC M30, M40, M60–ohv diagnostic. Available from: http://www.ohv-diagnostic.com/assets/project_components/media/documents/leaflets/EN/LL_M30M60_en_1.pdf. Accessed 17 February 2023

How to cite this article: Yan, Y., Zhao, Y., Zhao, K., Trinchero, R., Stievano, I.S., Li, H.: A high-efficiency portable system for insulation condition assessment of wind farm inter-array cables with double-sided partial discharge detection and localisation. IET Gener. Transm. Distrib. 17, 2523–2534 (2023). https://doi.org/10.1049/gtd2.12834

17518695, 2023, 11, Downloaded from https://ietresearch.onlinelibrary.wiley.com/doi/10.1049/gtd2.12834 by Politecnico Di Torino Sist. Bibl Del Polit Di Torino, Wiley Online Library on [16/06/2023]. See the Terms and Conditions (https://onlinelibrary.wiley.com/terms-and-conditions) on Wiley Online Library for rules of use; OA articles are governed by the applicable Creative Commons License